

PLAQUE IMAGING

## Quantification of Atherosclerosis with MRI and Image Processing in Spontaneously Hyperlipidemic Rabbits

Mari Hänni,\* H. Edvardsson, M. Wågberg, K. Pettersson,  
and Ö. Smedby

Department of Radiology, University Hospital, Uppsala, Sweden

### ABSTRACT

The need for a quantitative method to assess atherosclerosis in vivo is well known. This study tested, in a familiar animal model of atherosclerosis, a combination of magnetic resonance imaging (MRI) and image processing. Six spontaneously hyperlipidemic (Watanabe) rabbits were examined with a knee coil in a 1.5-T clinical MRI scanner. Inflow angio (2DI) and proton density weighted (PDW) images were acquired to examine 10 cm of the aorta immediately cranial to the aortic bifurcation. Examination of the thoracic aorta was added in four animals. To identify the inner and outer boundary of the arterial wall, a dynamic contour algorithm (Gradient Vector Flow snakes) was applied to the 2DI and PDW images, respectively, after which the vessel wall area was calculated. The results were compared with histopathological measurements of intima and intima-media cross-sectional area. The correlation coefficient between wall area measurements with MRI snakes and intima-media area was 0.879 when computed individual-wise for abdominal aortas, 0.958 for thoracic aortas, and 0.834 when computed segment-wise. When the algorithm was applied to the PDW images only, somewhat lower correlations were obtained. The MRI yielded significantly higher values than histopathology, which excludes the adventitia. Magnetic resonance imaging, in combination with dynamic contours, may be a suitable technique for quantitative assessment of atherosclerosis in vivo. Using two sequences for the measurement seems to be superior to using a single sequence.

*Key Words:* Atherosclerosis; Quantification; Magnetic resonance; Image processing; Animal model.

---

\*Correspondence: Mari Hänni, Department of Radiology, University Hospital, SE-751 85 Uppsala, Sweden; E-mail: mari.hanni@rtg.uas.lul.se.

## INTRODUCTION

In the evaluation of new drugs to combat atherosclerosis, there is a need for methods with which to quantify plaques, that can be used *in vivo* to monitor the same animal or patient. Magnetic resonance imaging (MRI) is a noninvasive method that can be used to assess atherosclerosis (Skinner et al., 1995; Yuan et al., 1996). In an earlier article, we proposed a quantitative method based on a combination of MRI and image processing techniques [thresholding and three-dimensional (3D) morphology] (Hänni et al., 1999). Using cholesterol-fed New Zealand White rabbits, it was found that the technique could distinguish between healthy and severely atherosclerotic aortas, but no correlation to postmortem findings was made. Because the MR signal can vary between individual animals and within the examined volume, it was necessary to select threshold values in a rather subjective way. The procedure was also rather time-consuming.

The purpose of this study was to evaluate two modifications of our method, by using the same MRI protocol but other image-processing techniques, in a different animal model, and to correlate the results with histopathologic analysis.

## MATERIAL AND METHODS

Six spontaneously hyperlipidemic (Watanabe) rabbits, approximately 18 months old and weighing 4.0–4.5 kg, were examined with a Philips Gyroscan ACS NT-II imager with a field strength of 1.5 T using a knee coil. The animals had not undergone any treatment that might have affected the development of atherosclerosis. They were anesthetized with a mixture of ketamine (50 mg/mL) and xylazine (20 mg/mL) administered by repeated *i.v.* injection during the scanning.

The MRI protocol for the abdominal aorta was identical to that used in our earlier study (Hänni et al., 1999), so that the 10-cm segment located immediately cranial to the aortic bifurcation was included (Table 1). To define the region of interest, we used three survey sequences. The first two showed the location of the aorta, and the third was used to locate the aortic bifurcation. The survey sequences were followed by an inflow angiography sequence (2DI) and a proton density weighted sequence (PDW), each consisting of 33 transverse slices. The PDW sequence, a turbo spin echo sequence, was applied in two consecutive acquisitions, the second filling the gaps in the first acquisition. The 2DI sequence, used for demarcation of the vessel wall inner boundary, showed the flowing

blood in the vessel with high signal intensity and the PDW, visualizing the surroundings with different intermediate signal intensities, was used for differentiating the outer wall boundary from adjacent tissues (Hänni et al., 1999). The in-plane voxel size (in the reconstructed images) of both sequences was 195  $\mu\text{m}$  and the slice thickness was 3 mm.

In four of the animals the thoracic aorta was also examined. The region of interest in the thoracic aorta was defined as 10 cm immediately cranial to the right renal artery. To reduce the scanning time, the PDW sequence was performed only once, producing 17 slices with a 3-mm gap.

To measure the thickness of the aortic wall, we used a Gradient Vector Flow (GVF) snake algorithm, developed by Xu and Prince (1988), which was applied to the 2DI and PDW images. The snake is a dynamic contour that is attracted to regions in the image that are rich in edge information (Kass et al., 1987) (cf. Fig. 1). When the snake is applied to the MRI slices, it will seek the borders between tissues that differ in signal, such as the inner and outer border of the vessel wall in the 2DI and PDW images, respectively. The flowing blood in the 2DI images is shown with high signal intensity, consequently, the edge information is high in the region of the images where the boundary between flowing blood and stationary tissue is located. A complete program for dealing with and segmenting the images was implemented in the Matlab language (MathWorks, Inc.) and run on a Sun Ultra 30 workstation (Sun Microsystems Comp).

When segmenting the slices, we started with the 2DI images. An initial approximation by four different points was manually set close to the region where the high signal is located in the 2DI images and the snake algorithm was initiated (Fig. 2). The starting points were applied on the 2DI slice located cranial to the aortic bifurcation. For each animal, only the 2DI image cranial to the aortic bifurcation was used to set the starting points. When the snake converged (the typical computation time was approximately 1 sec), the final curve was used as an initial approximation in the subsequent slice. If the algorithm made an obvious mistake (which happened in approximately 10% of the slices that were analyzed), the operator could interactively correct this. This operation was repeated throughout the volume, producing one curve for the inner wall boundary in each slice. In the first slice, the curve from the 2DI was then used as initialization curve in the PDW image. In subsequent PDW slices, the contour from the previous PDW slice was used for initialization. However, there are two edges present in the PDW images: one between the lumen and the



**Table 1.** MRI protocol.

| Sequence type          | Survey 1             |                    | Survey 2          |                                     | Survey PC                        |   | Survey 2DI      |                 | 2DI abdominal aorta |                 | PDW abdominal aorta |                 |
|------------------------|----------------------|--------------------|-------------------|-------------------------------------|----------------------------------|---|-----------------|-----------------|---------------------|-----------------|---------------------|-----------------|
|                        | Turbo spin echo      | Turbo spin echo    | Turbo spin echo   | Turbo spin echo                     | Fast field echo (Phase Contrast) | Fast field echo                             | Fast field echo | Fast field echo | Fast field echo     | Fast field echo | Turbo spin echo     | Turbo spin echo |
| Slices                 | 3 × 10 mm transverse | 3 × 10 mm sagittal | 1 × 70 mm coronal | 33 × 4 mm transverse (1 mm overlap) | 20 × 4 mm transverse             | 17 × 3 mm + 16 × 3 mm transverse (3 mm gap) |                 |                 |                     |                 |                     |                 |
| TR                     | 251 ms               | 251 ms             | 15 ms             | 47 ms                               | 24 ms                            | 2600 ms                                     |                 |                 |                     |                 |                     |                 |
| TE                     | 12 ms                | 12 ms              | 9 ms              | 10 ms                               | 6 ms                             | 18ms  |                 |                 |                     |                 |                     |                 |
| Turbo factor           | 6                    | 6                  | 20...             | 90...                               | 6                                | 5   |                 |                 |                     |                 |                     |                 |
| Flip angle             | 90...                | 90...              | 10 cm/sec         | 90...                               | 90...                            | 90...                                       |                 |                 |                     |                 |                     |                 |
| Velocity encoding      |                      |                    | 350 mm            |                                     |                                  |   |                 |                 |                     |                 |                     |                 |
| Field of view          | 300 mm               | 300 mm             | 256 × 256         | 256 × 256                           | 180 mm                           | 50 mm                                       |                 |                 |                     |                 |                     |                 |
| Acquisition matrix     | 256 × 256            | 256 × 256          | 256 × 256         | 256 × 256                           | 256 × 256                        | 128 × 256                                   |                 |                 |                     |                 |                     |                 |
| Reconstruction matrix  | 256 × 256            | 256 × 256          | 256 × 256         | 256 × 256                           | 256 × 256                        | 256 × 256                                   |                 |                 |                     |                 |                     |                 |
| Numbers of acquisition | 1                    | 1                  | 8                 | 2                                   | 2                                | 12  |                 |                 |                     |                 |                     |                 |
| Acquisition time       | 0:08                 | 0:08               | 0:31              | 1:35                                | 1:35                             | 2 × 8:50                                    |                 |                 |                     |                 |                     |                 |

A single application of the PDW sequence and a shortened 2DI sequence, 17 × 3 mm, were applied when the thoracic aorta was examined in four animals.



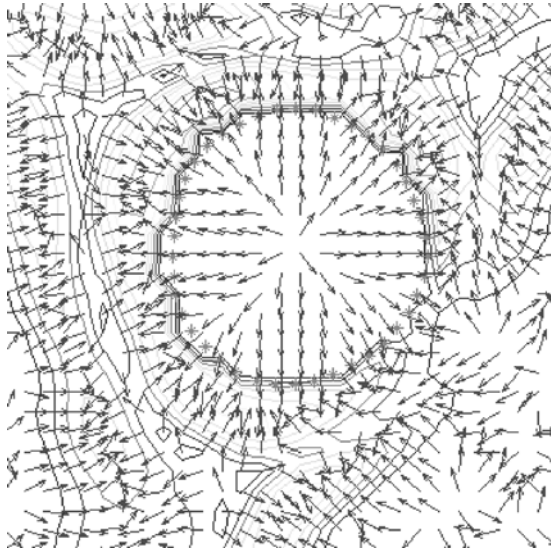


**Figure 1.** Gradient forces in a PDW image. The star line is indicating the position of the resulting snake in this image. The location is positioned automatically to the site where the inner forces of the snake and the outer forces originating from the edge information in the image are in balance. (View this art in color at [www.dekker.com](http://www.dekker.com).)

vessel wall and one between the vessel wall and the surrounding tissue (mostly fat). The first edge was identified in the 2DI images. By erasing the edge information in all pixels inside the region defined by the 2DI snake, it was possible to identify the remaining edge (i.e., the outer vessel wall boundary).

The alignment between the sequences was checked visually. When necessary, translation in the plane was performed, and the alignment was again checked visually. The total vessel volume, comprising vessel wall and lumen, as well as the vessel wall volume itself was computed from each slice. From the vessel wall volume and the area of the inner boundary, the average thickness of the vessel wall could be computed. The duration of the image processing, from initializing the snake in the first 2DI image until the vessel wall dimensions were finally calculated, was approximately 2 mins.

To test an alternative approach, the snake algorithm was also applied to the PDW images only for identification of both the inner and the outer vessel wall boundaries. The initial approximation was performed in the slice located proximal to the aortic bifurcation. The algorithm was started and the resulting snake was transported automatically to the subsequent image, where it was used as an initialization curve. The alignment between slices was checked visually, and when needed, a manual correction of the

initialization curve was performed. Two of the rabbits had changed the position during the scanning. The lumen area, vessel wall thickness, and area were computed in each slice.

### Histopathology

After the final MRI examination, the animals were anesthetized with a lethal dose of methohexital (Brietal, Eli-Lilly), the chest and abdomen were opened, and the entire aorta was removed. Because the rabbit aorta is a highly elastic tissue and will shrink when removed, the vessel was prepared in situ. A 10-cm-long segment cranial to the aortic bifurcation and 10cm cranial to the right renal artery were marked before removal for histopathological analysis. The aortas were cleansed and then fixed in neutral-buffered 4% formaldehyde (NBF). The lengths of the segments were then again measured, and the cross-sectional areas measured were adjusted individually for the degree of shortening. The sections were stained with Weigert's hematoxylin-van Gieson stain. Each aortic segment was divided into 10 slices, from which 2- to 3- $\mu$ m-thick sections were cut and stained with Weigert's hematoxylin-van Gieson. Quantitation of cross-sectional areas of the aorta was obtained by planimetry, using a Lucivid device (MicroBrightField, Colchester, Vermont) attached to a Leitz DRM microscope. This device superimposed a computer-generated display onto the microscope image. The external elastic lamina and the luminal border were manually traced by using the mouse-operated cursor, and the wall cross-sectional area was obtained as the difference between the two areas enclosed. Intima cross-sectional area was obtained as the area confined by the internal elastic laminae minus the lumen area. Planimetry was performed by using Microvid Software (MikroMakro AB, Gothenburg, Sweden).

### Statistical Methods

The relationship between repeated MRI evaluations and between MRI (both sequences as well as PDW only) and histopathology was assessed by using Pearson correlation coefficient ( $r$ ). Differences in the levels measured by the two techniques were evaluated with Bland-Altman diagrams.

### RESULTS

To test the reproducibility of the method, the image analysis (using both PDW and 2DI images) was

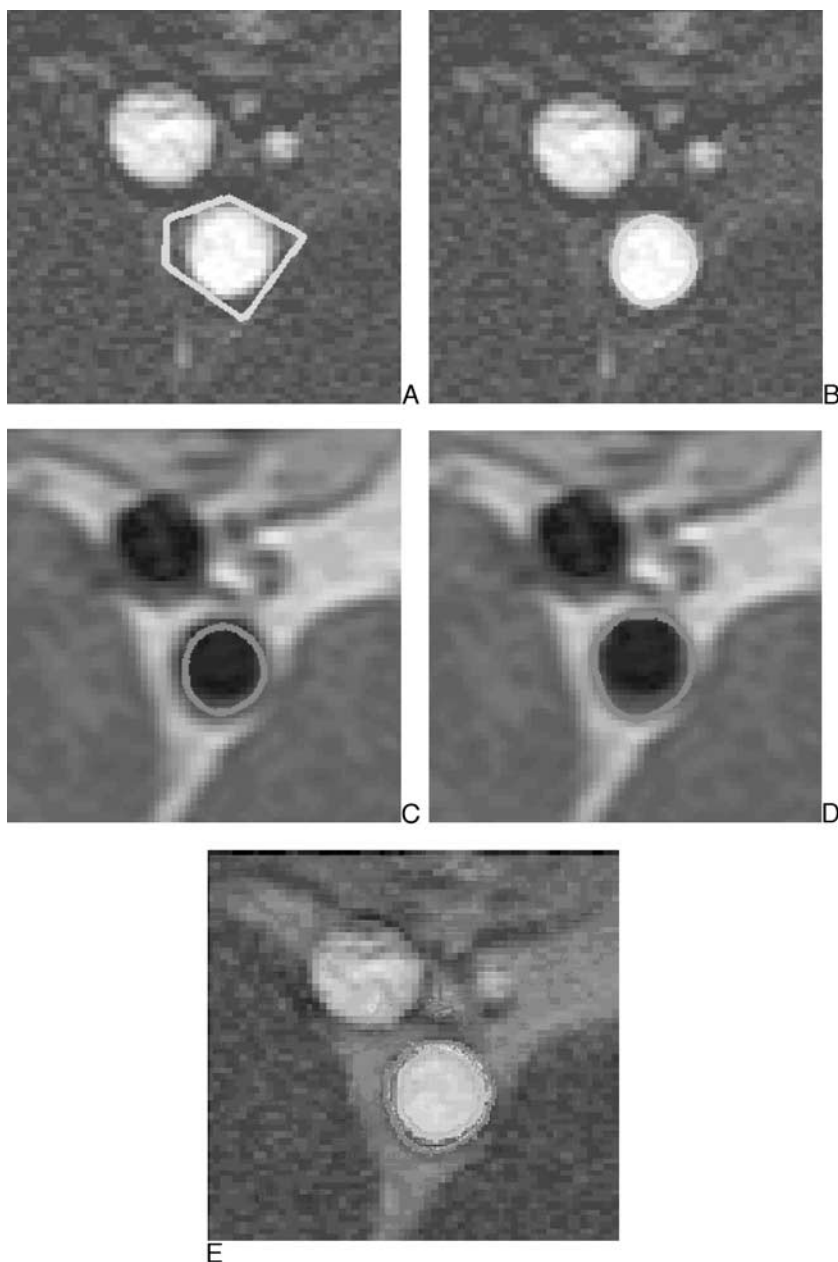


**Figure 2.** Example of the GVF snake algorithm. A coarse approximation is drawn in the first 2DI slice (A). The final position of the snake in this slice (B), corresponding to the inner boundary of the vessel wall, is transferred to the next 2DI slice and also to the first PDW slice (C). The final position of the snake in this image (D) represents the outer border of the vessel wall, and the area between the two snakes (E) is a measure of the wall thickness. (View this art in color at [www.dekker.com](http://www.dekker.com).)

performed three times by three independent observers. The correlation thus obtained was high (pairwise  $r = 0.909, 0.941, \text{ and } 0.949$ ).

The correlation between aorta cross-sectional areas measured with MRI (both sequences) and with histopathology (intima and media) was 0.879 for the six abdominal aortas and 0.958 for the four thoracic aortas. As seen in Fig. 3A, the MRI values, also including

the adventitia, were higher than the histopathology values. This difference was even more pronounced when only the intima was included in the histopathology results (cf. Fig. 3B,  $r = 0.902$  and  $0.947$ , respectively). The mean wall thickness measured with MRI displayed correlations of 0.863 and 0.827 with histopathological intima-media area and 0.926 and 0.775 with intima area.



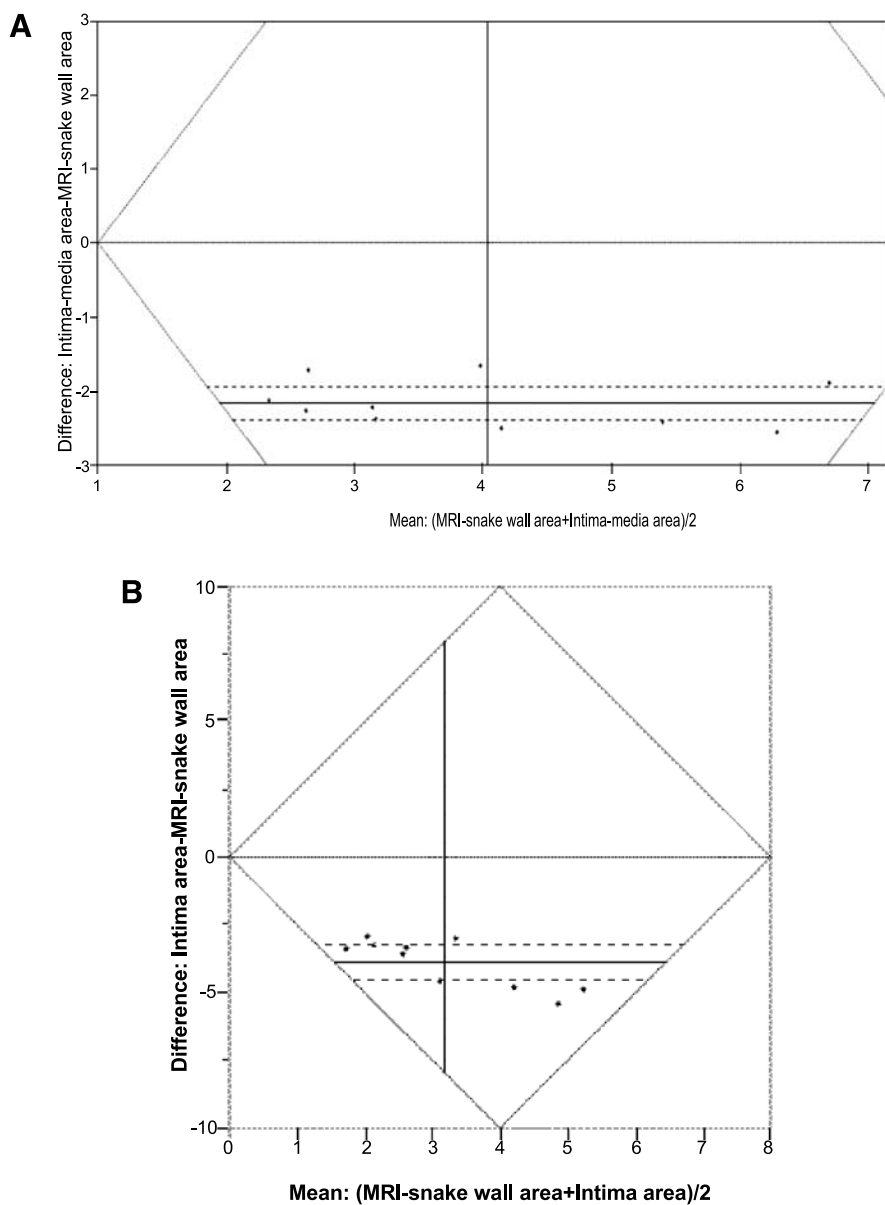


**Figure 3.** (A) Bland-Altman diagram relating MRI snake wall area to histopathological measurements of intima-media for 10 vessels (6 abdominal and 4 thoracic aortas). Mean difference:  $-2.2 \text{ mm}^2$  95% confidence limits:  $-2.4$  and  $-1.9 \text{ mm}^2$ . (B) Bland-Altman diagram relating MRI snake wall area to histopathological measurements of intima for 10 vessels. Mean difference:  $-3.9 \text{ mm}^2$  (95% confidence limits:  $-4.5$  and  $-3.2 \text{ mm}^2$ ).

The comparison of cross-sectional areas was repeated for the entire material, consisting of 99 vessel segments (each 10 mm long). Now, the correlation to MRI was 0.834 for intima-media and 0.753 for intima only, and the individual differences were greater even though the mean differences were unchanged (Fig. 4A and B). The wall area measured from the PDW sequences alone showed a segmentwise correlation of 0.663 with intima-media area and 0.592 with intima area.

## DISCUSSION

In this study we have used an approach to measure the arterial wall using in vivo MRI in combination with image processing. The scanning procedure was similar to what we used previously (Hänni et al., 1999), and by combining this protocol with a GVF snake algorithm, we could reliably measure vessel wall area non-invasively. Atherosclerosis is a disease affecting the



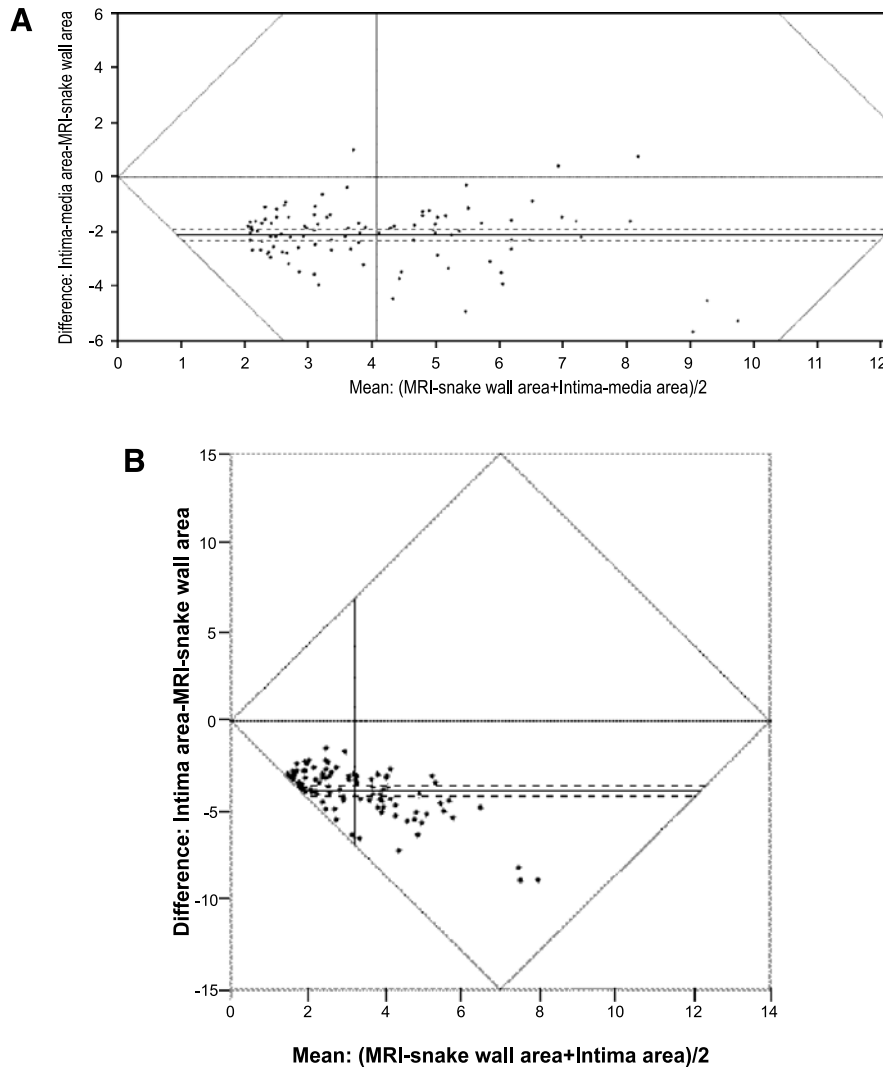


**Figure 4.** (A) Bland-Altman diagram relating MRI snake wall area to histopathological measurement of intima-media for 99 vessel segments. Mean difference:  $-2.1 \text{ mm}^2$  (95% confidence limits:  $-2.4$  and  $-1.9 \text{ mm}^2$ ). (B) Bland-Altman diagram relating MRI snake wall area to histopathological measurement of intima for 99 vessel segments. Mean difference:  $-3.9 \text{ mm}^2$  (95% confidence limits:  $-4.2$  and  $-3.6 \text{ mm}^2$ ).

arterial wall dimensions, (Glagov et al., 1987) and we were also able to show that the vessel wall area measured by MRI and GVF snakes was directly correlated to histopathological measurement of the sum of intima and media cross-sectional area.

Although some arterial sites are prone to atherosclerotic lesion development and other sites are more resistant, there is a large degree of variability between individuals concerning the exact location of the plaques. This is true both in man and in the rabbits used in this study. Our approach was, therefore, to develop a method that would not primarily identify the individual atherosclerotic plaque but, rather, result in a

measure of the thickening of the arterial wall. In an earlier attempt, we were able to demonstrate vessel wall thickening, compared to normal controls, after 6–7 months of cholesterol feeding to New Zealand White rabbits, but we did not perform any histological validation of the MRI measures obtained in that study (Hänni et al., 1999). The vessel wall area was measured by segmentation of different tissues, and the thresholding procedure is somewhat subjective because the threshold values have to be decided by the operator. We wanted to test a less operator-dependent method for image processing and simultaneously not as time-consuming as thresholding. The high correlation

between observers indicates that operator dependence is not a problem with the present method.

Our results show that cross-sectional wall area and wall thickness measured with MRI correlated significantly with histology wall area measures. Hence, they are closely related to the degree of atherosclerosis if a larger vessel wall area determined by histopathological measurements is considered to reflect the degree of atherosclerosis. The mean wall thickness could be an advantageous parameter to follow over time when longitudinal animal studies are performed, because it is less dependent on the size of the vessel.

The close correlation between MRI and histopathology remained true both when vessel wall area and thickness were evaluated in the caudal 10cm of the abdominal aorta and when using a simplified MRI protocol in the vessel segment containing the cranial part of abdominal aorta and the descending part of thoracic aorta. This latter part is subject to respiratory and cardiac motions and has been avoided in many studies (Fayad et al., 1998; Yuan et al., 1996). Our findings show that vessel wall can be measured by using MRI also in such locations, supporting the recent observations from Helft et al. (2001). In our experience, the motion artifacts mostly affect the PDW images. In our study, we have combined the PDW sequence with a 2DI sequence, which also facilitates measuring the vessel wall.

In addition to the general degree of the disease, it may be useful to be able to study differences in atherosclerotic involvement between sections of the aorta. Our segmentwise analyses (Fig. 4) show good correlation with histopathology also in this respect. In this study, the information from histopathology was somewhat limited in that only 10 slices, 2- to 3-mm thick from 10 levels in a 10-cm vessel segment were evaluated. It is not clear whether a more detailed histopathological analysis would reveal closer agreement or discrepancies due to noise in the MRI data. Another limitation of the present study is that perfusion fixation of the aortas was not used, which might have improved the accuracy of the histological measurements. In this study, we only wanted to measure the intima and the sum of intima and media area. Perfusion fixation is commonly used when vessel wall area is measured and compared with other methods. We did not perform perfusion fixation but a precise calculation of the degree of shrinkage. The degree of deformation does not affect the area measurements.

Recently, several studies have applied MRI for *in vivo* assessment of atherosclerosis (Fayad et al., 1998; Helft et al., 2001; Kang et al., 2000; Skinner et al., 1995; Yuan et al., 1996). Other studies have applied MRI in combination with a similar image-processing

technique (dynamic contour algorithms) for assessment of vessel wall area in healthy volunteers (Ladak et al., 2001). Our study differs from many earlier studies in the selection of MRI sequences and postprocessing methods. To achieve quantitative volume measurements, we used separate MRI sequences to identify the inner and outer boundaries of the arterial wall and combined them with the GVF Snakes algorithm. Apparently, this combination has not been used before in an animal model. The combination of two different MRI sequences may be a weakness of the method, because it requires good alignment between two image series, which is difficult after the examination. However, the results of this study indicate that the approach with two sets of images (2DI and PDW) gives results in closer agreement with histopathology than the alternative method, using PDW images only. Therefore, we have preferred to use an angiographic sequence as a more exact representation of the blood flow. The inflow angiographic sequence that we chose shows the flowing blood with high signal and the stationary tissue with low or no signal. When applying the GVF snake to the images, this fact is advantageous, because there is only one contour present in the 2DI images. The use of a PDW image series only often demands more extensive interaction by the operator who has to decide if intermediate signal in the vessel lumen or close to the vessel wall is due to turbulent blood flow, slowly flowing blood or a true vessel wall change. The use of fat saturation could be considered in the PDW sequence. With our approach, however, the contrast between fat with high signal and vessel wall with intermediate signal is essential for the identification of the outer boundary of the wall.

An attractive goal for MR imaging in atherosclerosis would be to image the plaques directly. However, because different plaques in the same individual can vary in chemical composition and, hence, in MR signal, it may be impossible to identify a certain signal pattern that characterizes all stages of the disease. Combining two sequences, we have used MRI to identify such tissues that are easily recognized with each sequence—flowing blood and surroundings—and whose characteristics are not expected to change during the course of the disease. Thus, the suggested method, which calculates the vessel wall area or thickness as the difference between inner and outer boundary, does not fail even when different kinds of plaque changes are present in the same arterial segment. On the other hand, the method, in its present form, does not give any information about plaque composition, which may be important to distinguish between stable and unstable plaques (Toussaint et al., 1996). Additional



MRI-sequences, T1-and T2-weighted sequences, would reveal information about the plaque composition. The goal in this study was limited to testing a quantitative noninvasive in vivo method to assess vessel wall dimensions.

Our study has shown that it is possible to use a clinical 1.5-T scanner and measure atherosclerotic vessel walls with results that agree closely with histopathology. However, an increase in field strength would probably improve the MRI examination's quality, and slice thickness could perhaps be reduced without losing resolution quality. This might be needed if animals with a smaller amount of vessel wall changes are studied. The actual slice thickness of 3 mm and an in-plane voxel size (in the reconstructed images) of 195  $\mu\text{m}$  appears to be sufficient in this animal model. It may be noted that in our implementation of the snakes algorithm, the position of the control points of the snake is given by floating-point coordinates, which enable us to some extent to compensate for partial volume effects.

Watanabe rabbits develop atherosclerosis from the age of 4 months and thereafter increasing with age. The lesions in the abdominal aorta most often consist of pronounced diffuse intimal thickening and fatty deposits (Hansen et al., 1994; Rosenfeld et al., 1987; Shiomi et al., 1992). In the thoracic aorta, there are more fatty streaks and fibrous lesions. In general, the wall changes in the thoracic aorta are more pronounced than in the abdominal aorta, as illustrated in Figs. 3 and 4. The animals in our study were about 18 months old and had developed moderate to severe vessel wall changes. In future studies, we intend to test the method's ability to detect more subtle atherosclerotic changes.

In conclusion, our study has shown that a combination of MRI and image-processing methods can be used to quantify atherosclerotic vessel wall changes, yielding results in close agreement with histopathology. A combination of two sequences seems superior to using a single sequence. In future studies, we will apply this method to study the progression or regression of vessel wall changes. It will be very interesting to ascertain the smallest extent of vessel wall changes that the MRI snakes method can detect and to compare the method with other noninvasive techniques.

#### ACKNOWLEDGMENTS

This study was supported by the Swedish Medical Research Council (MFR) (grant no. 10884), by the Swedish Heart-Lung Foundation, and by Astra-Zeneca.

#### REFERENCES

- Corti, R., Fayad, Z. A., Fuster, V., Worthley, S. G., Helft, G., Chesebro, J., Mercuri, M., Badimon, J. J. (2001 Jul 17). Effects of lipid-lowering by simvastatin on human atherosclerotic lesions: a longitudinal study by high-resolution, noninvasive magnetic resonance imaging. *Circulation* 104(3):249–252.
- Fayad, Z. A., Fallon, J. T., Shinnar, M., Wehrli, S., Dansky, H. M., Poon, M., Badimon, J. J., Charlton, S. A., Fisher, E. A., Breslow, J. L., Fuster, V. (1998 Oct. 13). Noninvasive in vivo high-resolution magnetic imaging of atherosclerotic lesions in genetically engineered mice. *Circulation* 98(15):1541–1547.
- Glagov, S., Weisenber, E., Zarins, C. K., Stankunavicius, R., Kolettis, G. J. (1987). Compensatory enlargement of human atherosclerotic coronary arteries. *N. Engl. J. Med.* 316:1371–1375.
- Hänni, M., Lekka-Banos, I., Nilsson, S., Häggroth, L., Smedby, Ö. (1999). Quantitation of atherosclerosis by magnetic resonance imaging and 3-D morphology operators. *Magn. Reson. Imaging* 17(4):585–591.
- Hansen, B. F., Mortensen, A., Hansen, J. F., Ibsen, P., Frandsen, H., Nordestgaard, B. G. (1994, Mar). Atherosclerosis in Watanabe heritable hyperlipidemic rabbits. Evaluation by macroscopic, microscopic and biochemical methods and comparison of atherosclerosis variables. *APMIS* 102(3):177–190.
- Helft, G., Worthley, S. G., Fuster, V., Zaman, A. G., Schechter, C., Osende, J. I., Rodriguez, O. J., Fayad, J. T., Badimon, J. J. (2001 Mar 15). Atherosclerotic aortic component quantification by noninvasive magnetic resonance imaging: an in vivo study in rabbits. *J. Am. Coll. Cardiol.* 37(4):1149–1154.
- Kang, X., Polissar, N., Han, C., Lin, E., Yuan, C. (2000). Analysis of the measurement precision of arterial lumen and wall areas using high-resolution MRI. *Magn. Reson. Imaging* 44:968–972.
- Kass, M., Witkin, A., Terzopoulos, D. (1987). Snakes: active contour models. *Int. J. Comput. Vis.* 1(4):321–331.
- Ladak, H., Thomas, J., Mitchell, J., Rutt, B., Steinman, D. (2001). A semi-automatic technique for measurement of arterial wall from black blood MRI. *Med. Phys.* 28:1098–1107.
- Manninen, H. I., Vanninen, R. L., Laitinen, M., Rasanen, H., Vainio, P., Luoma, J. S., Pakkanen, T., Tulla, H., Yla-Herttuala, S. (1998). Intravascular ultrasound and magnetic resonance imaging



- in the assessment of atherosclerotic lesions in rabbit aorta. Correlation to histopathologic findings. *Invest. Radiol.* 33(8):464–471.
- Nilsson, S., Berglund, I., Erikson, U., Högman, N., Johansson, J., Walldius, G. (1991). Atherosclerosis-related measures in digitized femoral arteriograms. *Acta Radiol.* 32(1):24–29.
- Rosenfeld, M. E., Tsukada, T., Chait, A., Bierman, E. L., Gown, A. M., Ross, R. (1987). Fatty streak expansion and maturation in Watanabe heritable hyperlipemic and comparably hypercholesterolemic fat-fed rabbits. *Arteriosclerosis* 7:24–34.
- Shiomi, M., Ito, T., Shirashi, M., Watanabe, Y. (1992, Sep). Inheritability of atherosclerosis and the role of lipoproteins as risk factors in the development of atherosclerosis in WHHL rabbits: risk factors related to coronary atherosclerosis are different from those related to aortic atherosclerosis. *Atherosclerosis* 96(1):43–52.
- Skinner, M. P., Yuan, C., Mitsumori, L., Hayes, C. E., Raines, E. W., Nelson, J. A., Ross, R. (1995). Serial magnetic resonance imaging of experimental atherosclerosis detects lesion fine structure, progression and complications in vivo. *Nat. Med.* 1(1):69–73.
- Sramek, A., Bosch, J. G., Reiber, J. H., Van Oostaten, J. A., Rosendaal, F. R. (2000, Dec). Ultrasound assessment of atherosclerotic vessel wall changes: reproducibility of intima-media thickness measurements in carotid and femoral arteries. *Invest. Radiol.* 35(12):699–706.
- Ståhlberg, F., Ericsson, A., Nordell, B., Thomsen, C., Henriksen, O., Persson, B. R. R. (1992). MR imaging, flow and motion. *Acta Radiol.* 33(3):179–200.
- Toussaint, J. F., LaMuraglia, G. M., Southern, J. F., Fuster, V., Kantor, H. L. (1996). Magnetic resonance images lipid, fibrous, calcified, hemorrhagic, and thrombotic components of human atherosclerosis in vivo. *Circulation* 94(5):932–938.
- Wendelhag, I., Gustavsson, T., Suurkula, M., Berglund, G., Wikstrand, J. (1991). Ultrasound measurement of wall thickness in the carotid artery: fundamental principles and description of a computerized analysing system. *Clin. Physiol.* 11(6):565–577.
- Xu, C. Y., Prince, J. L. (1998, March). Snakes, shapes and gradient vector flow. *IEEE Trans. Image Process.* 359–369.
- Yock, P. G., Linker, D. T., Angelsen, B. A. (1989). Two-dimensional intravascular ultrasound: technical development and initial clinical experience. *J. Am. Soc. Echocardiogr.* 2(4):296–304.
- Yuan, C., Skinner, M. P., Kaneko, E., Mitsumori, L., Hayes, C. E., Raines, E. W., Nelson, J. A., Ross, R. (1996). Magnetic resonance imaging to study lesions of atherosclerosis in the hyperlipidemic rabbit aorta. *Magn. Reson. Imaging* 14(1):93–102.



## **Request Permission or Order Reprints Instantly!**

Interested in copying and sharing this article? In most cases, U.S. Copyright Law requires that you get permission from the article's rightsholder before using copyrighted content.

All information and materials found in this article, including but not limited to text, trademarks, patents, logos, graphics and images (the "Materials"), are the copyrighted works and other forms of intellectual property of Marcel Dekker, Inc., or its licensors. All rights not expressly granted are reserved.

Get permission to lawfully reproduce and distribute the Materials or order reprints quickly and painlessly. Simply click on the "Request Permission/Order Reprints" link below and follow the instructions. Visit the [U.S. Copyright Office](#) for information on Fair Use limitations of U.S. copyright law. Please refer to The Association of American Publishers' (AAP) website for guidelines on [Fair Use in the Classroom](#).

The Materials are for your personal use only and cannot be reformatted, reposted, resold or distributed by electronic means or otherwise without permission from Marcel Dekker, Inc. Marcel Dekker, Inc. grants you the limited right to display the Materials only on your personal computer or personal wireless device, and to copy and download single copies of such Materials provided that any copyright, trademark or other notice appearing on such Materials is also retained by, displayed, copied or downloaded as part of the Materials and is not removed or obscured, and provided you do not edit, modify, alter or enhance the Materials. Please refer to our [Website User Agreement](#) for more details.

### **[Request Permission/Order Reprints](#)**

Reprints of this article can also be ordered at

<http://www.dekker.com/servlet/product/DOI/101081JCMR120038087>